ICARUS 50, 288–310 (1982)

Martian Great Dust Storms: An Update

RICHARD W. ZUREK

Jet Propulsion Laboratory, T-1166, California Institute of Technology, Pasadena, California 91109

Received November 2, 1981; revised March 3, 1982

Observations by the Viking Orbiters and Landers have made substantial contributions to our understanding of the episodic, planetary-scale dust storms on Mars. These and other observations pertinent to the great dust storms are reviewed in this paper; most of the emphasis is on the atmospheric/climatic aspects of these great storms. Specifically, observations concerning the optical properties of the airborne dust, the frequency of occurrence of great dust storms, and the kinematics of their evolution are summarized. Special attention is given to the various estimates derived from Viking data of atmospheric dust opacity. Within this observational framework, various physical mechanisms underlying the generation, evolution, and decay of the Martian great dust storms are discussed.

INTRODUCTION

Assuming that the polar laminae represent a depositional record reflecting climatic change on Mars, the proper interpretation of that record will require an understanding of the long-term cycles of the generation, transport, and deposition of airborne dust. Our characterization of these long-term dust cycles is necessarily based on observations of the seasonal dust cycle on Mars and its interannual variability. These, in turn, are dominated by the great dust storms, which extend over vast areas and involve large volumes of material.

Since the review by Gierasch (1974), observations by the Viking spacecraft have added greatly to our understanding of Martian dust storms. Much of this new material and the theoretical studies generated by it is contained in the collection of papers published as a special issue of the *Journal of Geophysical Research* (Vol. 84, June 10, 1979, pp. 2793–3007). Some of the more recent work is cited here, although this review will concentrate on the atmospheric and climatic aspects of the Martian great dust storms. The early sections will summarize, hopefully in an objective manner, our present knowledge of the characteristic opacity history and of the frequency of the great dust storms. Because of their importance to dynamical modeling of the great storms, the opacity and the optical constants needed to compute the thermodynamic effects of the Martian airborne dust will be discussed at some length. Composition of the dust and its fate while on the Martian surface will be largely neglected; the interested reader is referred elsewhere (Pollack *et al.*, 1977, 1979; Veverka *et al.*, 1981; Peterfreund, 1981). The concluding sections discuss our present understanding of dust-storm generation and evolution, again with some emphasis on the climatic aspects; these sections are necessarily more speculative.

OPACITY

The evolution, scale, and intensity of a Martian great dust storm is defined primarily in terms of the opacity of the dust it raises. "Great" storms are those which obscure planetary-scale sections of the Martian surface for many Martian days (sols). Based on Mariner 9 and Viking observations, various studies have attempted to quantitatively define the opacity (τ) of the dust-laden atmosphere during a great dust

Presented at the "Workshop on Quasi-Periodic Climatic Changes on Earth and Mars" held at NASA's Ames Research Center, Moffett Field, California, February 24–26, 1981.

0019-1035/82/050288-23$02.00/0

storm. These studies[1] can be divided as follows. Estimates based directly on remotely observed radiances include studies which use: (1) Viking Lander images of the Sun and Phobos (Pollack *et al.*, 1977, 1979; Kahn *et al.*, 1981), (2) Orbiter (TV) images of the surface or the limb of the planet (Thorpe, 1973, 1979, 1981; Leovy *et al.*, 1972; Anderson and Leovy, 1978), and (3) Orbiter infrared observations (Toon *et al.*, 1977; Martin *et al.*, 1979; Hunt *et al.*, 1980; Pleskot and Miner, 1981). Less direct estimates of atmospheric dust opacities have used such geophysical fields as atmospheric temperature (Gierasch and Goody, 1972; Conrath, 1975; Leovy and Zurek, 1979) and surface pressure (Zurek, 1981).

The most reliable of these estimates is probably that derived by Pollack *et al.* (1977, 1979) from images taken of the Sun and Phobos with a special diode on the Viking Lander cameras. Since the cameras are sitting on the Martian surface, the measured intensity I is directly related by Beer's law to the optical depth of the intervening atmospheric haze:

$$I = I_0 \exp\,[-\tau/M(\epsilon)].$$

I_0 is the unattenuated intensity at the top of the atmosphere, and $M(\epsilon)$ is the airmass determined by the elevation angle ϵ. By ratioing pairs of images taken close together in time but with different elevation angles, τ can be determined subject only to errors in ϵ (estimated to be a few tenths of a degree) and to measurement errors (including both calibration and digitization). When pairs of images could not be obtained at a given time, optical depths could sometimes be derived using single images and an I_0 value computed from pairs of images taken at a different time on the same day and with the same diode. Unlike methods which deal with solar reflected or thermally emitted radiation, this method is independent of the optical properties and temperature of the ground and airborne dust. However, the Lander cameras cannot look overhead and opacities have to be derived for large airmasses. Most estimates were made 1 or 2 hr before sunset or after sunrise; those estimates which were made during the day or during periods of large opacity ($\tau > 2$) usually suffered from low signal-to-noise ratios.

Figure 1 shows the extinction optical depths τ (for visible, vertically incident insolation) derived from the Viking Lander imaging data taken from the surface of Mars during the first Martian year of observations.[2] Three items are immediately noteworthy: (1) the opacity increases sharply to large values ($\tau > 2$) at Lander 1 near L_S = 205 and 279°, (2) the opacities at the two Lander sites (VL1 at 22.5°N, 48°W; VL2 at 48°N, 226°W) have similar trends but τ is generally smaller at the more northern site, and (3) the opacity never seems to fall below a value of a few tenths at any time during the year. Since there are only two Landers on Mars, both resting in low-lying basins in the northern hemisphere, the opacity curves shown in Fig. 1 cannot immediately be taken as representative of all locations on the planet. The most ambitious of the attempts to quantify the opacity histories for large areas of Mars have been the analyses by Thorpe (1979, 1981), who modeled observations taken by cameras onboard the Viking Orbiters of changing surficial feature contrasts. This was done by selecting features whose contrasts were due to surface relief (e.g., crater wall) and not to albedo. The surface phase function was modeled using the observed variation with phase angle of the radiance measured when atmospheric opacity was judged to be negligible. The radiance observed for the same scene in the presence of a dust haze and for the same viewing geometry was then mod-

[1] The quantitative determination of τ is emphasized here; many other studies have dealt with the detection and effects of Martian dust hazes and storms.

[2] The seasonal date is given in terms of L_S, the longitude of the Sun in Mars-centered (areocentric) coordinates. L_S = 0° = 360° corresponds to spring equinox in the northern hemisphere.

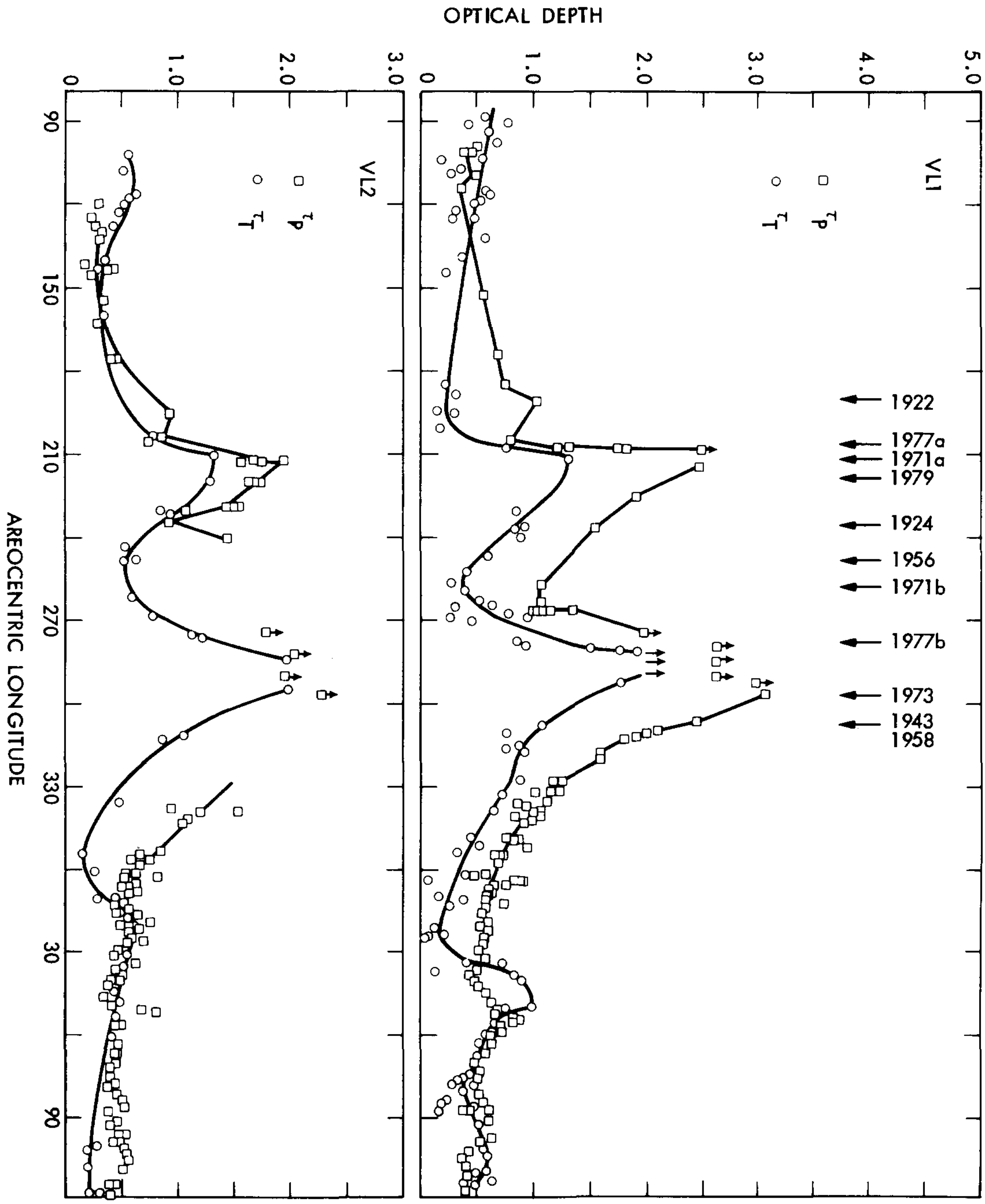

FIG. 1. Normal-incidence optical depth τ of the dust haze above Viking Lander 1 (top) and Lander 2 (bottom) as a function of areocentric longitude L_S (L_S = 90 and 270° corresponding to northern and southern summer solstices, respectively) for the first Mars year of Viking observations. The τ_P values are the afternoon values determined by Pollack *et al.* (1979) from imaging the Sun's disk with the Viking Lander imaging systems. The τ_T values are computed by Thorpe (1981) from modeling the scene reflectance and contrast modulation observed with the Viking Orbiter cameras using red and clear filters. Arrows mark periods when only lower bounds to the τ_P, τ_T values were estimated. The L_S values for the observed onsets of great dust storms on Mars (identified by the year in which they occurred) are also marked.

eled by separating the radiance to be measured at the spacecraft into three components (Van Blerkom, 1971): (i) I_{AS}, the direct sunlight reflected from the haze alone, (ii) I_{MS}, that sunlight transmitted directly and by scattering to the surface where it is reflected to the spacecraft without further scattering, and (iii) I_{MAS}, the sunlight reflected off the surface in all other directions, but which is subsequently scattered toward the spacecraft by the haze. This last term gives rise to a blurring of surface detail as photons which were reflected from the surface of one region are scattered in the haze above the adjacent region toward the spacecraft. For the atmospheric haze, Thorpe (1979, 1981) used a Henyey–Greenstein phase function in a single-scattering approximation modified by a correction factor designed to include the effects of higher-order scattering. When computing the term I_{MAS}, the dust haze is assumed to be a single-scattering layer concentrated at altitude H. The resulting model predicts for the geometry of each scene the reflectance of the scene and the modulation (i.e., the normalized contrast as a function of distance from the contrast boundary) as functions of opacity τ, single-scattering albedo $\tilde{\omega}_0$, phase function asymmetry parameter g, and dust cloud height H. In practice, Thorpe sets $\tilde{\omega}_0 = 0.85$ based on Viking Orbiter observations of the Mars opposition effect (Thorpe, 1978), and the model results are not sensitive to $H \gtrsim 1$ km. Otherwise, τ and g are incremented until both the reflectance and the modulation computed by the model match the observations to within given bounds (e.g., $\pm 30\%$).

As the above discussion implies, the analysis of the Orbiter imaging data is highly model dependent. Recently, Thorpe has applied his approach to Orbiter visual imaging of the Viking Lander sites, and his results (taken from Thorpe, 1981) are compared in Fig. 1 to those optical depths computed by Pollack *et al.* (1977, 1979) from the Lander imaging data. These two derivations agree early and late in the Viking mission but, as shown in Fig. 2, Thorpe's (1981) values are smaller by nearly a factor of 2 during the interim, when dust opacities were largest. The size and consistency of this difference cannot be explained in terms of a diurnal variation of the atmospheric opacity above the Lander sites, since it is highly improbable that condensate hazes or fogs would form near the terminator with the same opacity as the dust haze, even as that opacity changed from day to day, only to completely disappear during most of the day. This is not to say that atmospheric condensates are not present. Opacities measured after sunrise are often observed to be higher than afternoon opacities by $\Delta\tau \sim 0.2$–0.6 (Pollack *et al.*, 1977, 1979), but this is much too small to account for the discrepancy shown in Fig. 1. Night-time opacities estimated at $L_S = 129°$ from Viking Lander 2 imaging of Phobos indicated that this opacity increase occurs largely in the early morning hours before sunrise and is consistent with the night-time formation of a ground fog. There was no evidence of a similar condensate haze during the late afternoon measurements.

Certainly, the single-scattering framework used by Thorpe (1979) is less valid for large optical depths, as multiple-scattering effects become important. Thorpe's (1981) parametric studies of scene contrasts indicate that there may be more than one pair of τ, g parameters which can yield essentially the same scene contrast when the optical depth is large ($\tau > 1$). It is noteworthy that an analysis of the Lander images of the brightness of the dusty atmosphere taken soon after the arrival of Lander 1 (Pollack *et al.*, 1977) yielded $\tilde{\omega}_0$ values close to those obtained by Thorpe (1978) from Orbiter imaging (0.86 compared to 0.8–0.85), but led to larger values of g (0.79 compared to g $\lesssim 0.6$).[3] The delta-Eddington scaling relations for the computation of radiative flux in a multiple-scattering medium (Joseph *et*

[3] The estimate of g from the Lander imaging data is far more model dependent than the estimate of τ.

al., 1976) suggest that the opacity τ_e derived using a less forward scattering approximation (in this case the Eddington approximation) is related to the more forward-scattering (delta-Eddington) case by

$$\tau/\tau_e \sim (1 - g^2\tilde{\omega}_0)^{-1} \sim 1.9$$

for $g = 0.79$. While more detailed calculations are required to truly test the hypothesis of multiple solutions, this simple scaling argument suggests that underestimating g can lead to a significant underestimate of τ.

Dust opacities estimated from Viking Orbiter Infrared Thermal Mapper (IRTM) radiance data also provide global coverage (Martin *et al.*, 1979). The opacities (at a wavelength of 9 μm) shown in Fig. 2 were derived by estimating the vertical-viewing values of the radiances in the 7-, 9-, and 15-μm IRTM channels from emission phase function sequences in which the same area was repeatedly viewed at different emission angles as the spacecraft flew overhead. Observations of the 1971 great dust storm by the Mariner 9 Infrared Interferometer Spectrometer (IRIS) indicated that the airborne dust had a strong, broad, well-defined absorption band at 9 μm (Hanel *et al.* 1972; Martin *et al.*, 1979), so the 9-μm radiance is the best indicator of the presence of atmospheric dust. Assuming that scattering can be neglected at these wavelengths, that the atmosphere is isothermal at the brightness temperature of the 15-μm CO_2 channel, and that the 7-μm radiance is largely unaffected by atmospheric dust, the opacity at 9 μm can be readily computed. The opacities shown in Fig. 2 were derived for a number of sites in the Martian low latitudes, and they have all been scaled to the altitude of the Viking Lander 1 site by assuming that the dust was uniformly mixed with height. For comparison in Fig. 2 with the opacities at visible wavelengths the 9-μm opacities have been arbitrarily scaled by a factor of 2.5. The scale factor was chosen to reproduce the visible opacity of the dust haze as seen from Lander 1 at $L_S \sim 226°$ during the decay phase of the first 1977 great dust storm. This factor represents not only the ratio of different extinction efficiencies at visible and infrared wavelengths, but also a correction factor for the model's many assumptions, such as the neglect of scattering in the dust haze. As shown, the trends of the 9-μm opacity during the two great dust storms of 1977 are very similar to those outlined by the visible imaging data at the Lander 1 site, suggesting that the dust haze is more or less uniformly dispersed over at least the Martian low latitudes during the great dust storms. There is also some suggestion that opacities at the Lander sites before the great dust storms were somewhat higher than those over upland regions, even when adjusted for the altitude difference.

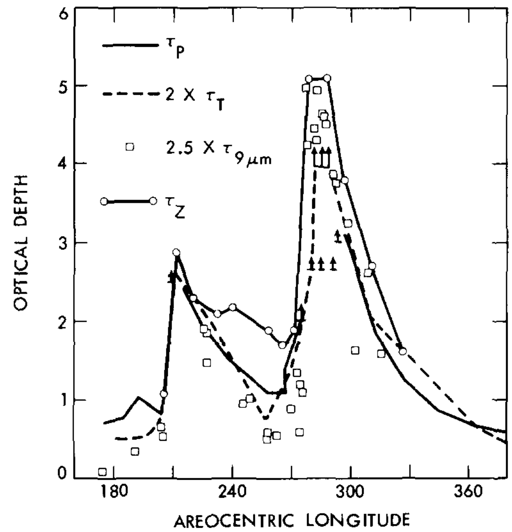

FIG. 2. Normal-incidence optical depths for the two 1977 Martian great dust storms as computed by Pollack *et al.* (1979) from the Viking Lander 1 imaging data (τ_P), by Thorpe (1981) from Viking Orbiter viewing of the Lander 1 sites (τ_T), by Martin *et al.* (1979) from Viking Orbiter Infrared Thermal Mapper phase function observations of low-latitude sites ($\tau_{9\,\mu m}$), and by Zurek (1981) from Lander 1 surface pressure data (τ_Z). $\tau_{9\,\mu m}$ values represent optical depths at infrared (9 μm) wavelengths; all other values are for visible (~0.6 μm) wavelengths. τ_Z values were computed for the L_S periods indicated by the circles. $\tau_{9\,\mu m}$ and τ_T values have been scaled as shown. See the text for further details.

The infrared opacities quoted here are being recomputed with a model which includes the effects of scattering, of nonisothermal atmospheres, and of wavelength-dependent surface emissivities. The variation of surface emissivity with wavelength has been parameterized in terms of surface (visible) albedo using an empirical correlation derived from the analysis of the diurnal variation of the four different surface-sensing IRTM channels (Christensen, 1982). Scattering effects are included via a delta-Eddington radiation code which uses the optical constants (of montmorillonite sample 219b) and the particle size distribution found by Toon *et al.* (1977) to be consistent with the Mariner 9 IRIS observations of the 1971 great dust storm. Preliminary results (Martin and Zurek, 1982) indicate that the inclusion of scattering effects and of more realistic (nonisothermal) temperature profiles tends to compensate one another so that the new estimates of opacities at 9 μm are only about 35% larger than the old. This suggests that the ratio of 9-μm to visible opacities (or equivalently, the ratio of the extinction factors Q_{EXT} appropriate to each wavelength) is 1.85 (= 2.5/1.35) for the opacities derived by Pollack *et al.* (1979) or 0.93 for those derived by Thorpe (1982). Based on an analysis of the sky brightness observed near the Sun's image by the Viking Lander cameras, Pollack *et al.* (1979) estimated $Q_{\mathrm{EXT}} \sim 2.74$ at visible wavelengths. For the same size distribution and for montmorillonite 219b, $Q_{\mathrm{EXT}} \sim 2.26$ at 9 μm (2.17 for basalt), so

$$\tau_{\mathrm{vis}}/\tau_{9\,\mu\mathrm{m}} \sim Q_{\mathrm{EXT(vis)}}/Q_{\mathrm{EXT}(9\,\mu\mathrm{m})} \sim 1.2.$$

To change this factor to 1.85 [0.93] by changing the particle size distribution would require an increase [decrease] of the average cross-section weighted particle radius on the order of 25% [14%] at 9 μm or a corresponding decrease [increase] of the effective radius at visible wavelengths. At present, one cannot choose between these possibilities given the uncertainty of the various model fits.

The last set of opacities shown in Fig. 2 was derived in quite a different way. Observations of the near-surface winds and pressure oscillations by the Viking Lander meteorological instruments indicated that the measured amplitudes of the thermally driven, planetary-scale atmospheric tides were closely coupled to the dust content of the Martian atmosphere, especially during great dust storms (Leovy and Zurek, 1979). Zurek (1981) used a delta-Eddington radiative transfer algorithm to compute the semidiurnal (twice daily) component of the solar heating of a Martian dust haze assumed to be uniformly distributed horizontally and up to several scale heights. The semidiurnal surface pressure response at the Viking Lander sites to this imposed solar heating was then computed using a classical atmospheric tidal model (Chapman and Lindzen, 1970). For a single-scattering albedo $\tilde{\omega}_0 =$ 0.86 and a phase function asymmetry parameter of $g = 0.5$ during dust storm onset and $g = 0.79$ elsewhere (see below) the (visual) opacities shown in Fig. 2 not only reproduced the semidiurnal pressure component at Lander 1 (Zurek, 1981), as they were designed to do, but also yielded reasonably good fits to all the tidal components observed at both Landers during the two 1977 great dust storms (Zurek and Leovy, 1981). As shown by Fig. 2, the opacities inferred from the Lander pressure data are most consistent with the opacities derived by Pollack *et al.* (1979). Because the horizontal scale of the atmospheric tidal pressure variation is comparable to the planetary radius, the opacities inferred from the Lander pressure data reflect the average opacity covering the Martian low latitudes (i.e., $\pm 40°$). The greatest uncertainties in the radiative-dynamic tidal model result from the neglect of tidal heating due to the convective heat flux from the surface (a good assumption during periods of large atmospheric dust opacities) and of the sizeable planetary-scale surface relief, plus the lack of details about the vertical distributions of temperature and dust mixing ratio. Changes in g (from 0.5 to 0.79) or in temperature (isothermal to nonisothermal) alter the values of τ needed to reproduce the observed semidiurnal surface pressure oscillation by up to 25%. Despite this sensitivity, the amplitudes of the semidiurnal and diurnal tides observed at Lander 1 during the periods $L_S \sim 205-230°$ and $275-310°$ are simply too large to be reproduced for optical depths as low ($\tau < 2$) as those derived by Thorpe (1981).

Although they are both highly model dependent, opacity estimates based on the Viking IRTM radiances and the Lander surface pressure data indicate that the opacity of the dust haze above Viking Lander 1 is fairly representative of the widespread dust haze over the Martian low latitudes during periods of large opacity (i.e., the great dust storms). Certainly, local variations have been observed even during great dust storms, and the general degree of atmospheric dustiness varies from storm to storm. The first storm observed by Viking, for instance, was not as extensive or as uniformly dusty over the regions it did cover as was the second. This is apparent in the visual photomosaics themselves (Briggs *et al.* 1979; Thorpe, 1979). The opacities derived for the southern hemisphere by Thorpe (1979) also show considerable spatial variation and a tendency for the largest opacities to occur between latitudes 30 and 50°S. The difficulties inherent in the analysis of the orbiter images—the single-scattering framework, the need for clear reference frames to define the surface phase function, the sensitivity to particle-dependent parameters—have been discussed above. However, the comparison of opacities shown in Fig. 1 indicates that the method does have some skill in predicting trends, if not the values, of opacity during the great dust storms. Figure 1 also illustrates the danger here: the large opacity increase computed by Thorpe (1981) for Lander 1 at $L_S \sim 40°$, suggesting a dust storm event almost on the scale of the first dust storm observed by Viking, is not seen in any of the Lander imaging or meteorological data.

DUST OPTICAL PARAMETERS

In addition to opacity, the calculation of radiative fluxes in a dusty Martian atmosphere requires at least the single-scattering albedos $\tilde{\omega}_0$ and phase function asymmetry parameters g for the relevant wavelengths. Thorpe (1978) used Viking Orbiter observations of the Mars opposition effect to estimate $\tilde{\omega}_0 = 0.80-0.85$ at 0.6 μm and 0.5 at 0.44 μm for dust storm conditions. Pollack *et al.* (1979) used the optical depths derived from the Sun diode images in an analysis of the angular variation of the sky brightness observed prior to the 1977 great dust storms to estimate the size, nonspherical shape, and complex refractive index of the dust particles. From this information they computed an effective (i.e., averaged over the solar spectrum) $\tilde{\omega}_0 = 0.86$ and $g = 0.79$ ($g = 1$ if the scattering is all in the forward direction). Using the method described in the previous section, Thorpe (1979, 1981) found values of g ranging from 0.0 (isotropic scattering) to 0.6. Both Thorpe (1978) and Pollack *et al.* (1977, 1979) found evidence suggesting the dust particles were nonspherical and that the effects of this nonspherical shape were optically important at visible and shorter wavelengths. The Lander imaging sky brightness data indicated relatively smooth particles having the platelike shape of typical clay particles.

The average cross-section weighted particle radius derived by Pollack *et al.* (1979) was $\bar{r} = 2.5$ μm for a modified gamma function particle size distribution. This was the same result obtained by Toon *et al.* (1977) in their modeling of the Mariner 9 IRIS observations of the 1971b dust storm. The estimate of similar size parameters for the dust raised in the 1971 and prior to the first 1977 great dust storm suggests that the same-sized particles tend to remain in the atmosphere after any dust event. At least it seems unlikely that the airborne dust above the Landers early in the Viking mission was the remnant of some previous great dust storm. The particles most likely to be moved at the ground beneath the thin Martian atmosphere are much larger ($\sim$100 μm in radius, Greeley *et al.*, 1980). Saltation of these larger particles will raise smaller particles from the surface, the largest of which will soon return because of gravitational setting. Analyses (Conrath, 1975; Toon *et al.*, 1977) of the Mariner 9 IRIS data indicated that the size distribution of particles in the range 1–10 μm remained essentially unchanged during the long decay phase of the 1971b great dust storm. The size distributions of the airborne dust during the early phases of a great dust storm or during a local storm are essentially unknown. However, R. Kahn reported (in an unpublished study) that the infrared opacities derived by using a two-stream radiative transfer code to model the Viking IRTM observations of the dust haze surrounding a local dust storm occurring in Solis Planum at L_S = 227° were *not* consistent with the infrared optical parameters obtained by Toon *et al.* (1977) from their analysis of the Mariner 9 IRIS data. Whether this was due to different particle sizes or to different composition was not determined.

Thorpe's (1981) analysis of Orbiter images of the Viking Lander 1 site suggested an increase in forward scattering by the dust during the onset of the 1977b storm (g = 0.2 to 0.6) followed by a decrease a few weeks later to prestorm values, although one must recall the possibility of multiple solutions when τ is large. Zurek (1981) suggested that the onsets of both 1977 great dust storms were characterized by smaller asymmetry parameters (g = 0.5 as opposed to g = 0.79), but in the context of the coupled radiative-dynamic tidal model this change in g could have simulated changes in other parameters, such as a concentration of the dust aloft. To produce these smaller values of g by changing the particle size would require *smaller* particles during dust storm onset and would imply smaller $\tilde{\omega}_0$ as well, a change not indicated by either of the above analyses.

For particles characterized by $\bar{r} \sim 2$ μm, the radiative properties of the airborne dust at visible wavelengths can be dominated by quite minor constituents. Pang *et al.* (1976) and later Pang and Ajello (1977) used a single-scattering algorithm to match phase functions generated by a Mie scattering program to the ultraviolet reflectances observed during the 1971 great dust storm by the Mariner 9 Ultraviolet Spectrometer (UVS). They determined a mean particle size $\bar{r} \sim 1.5$ μm and ascribed the absorption feature observed in the ultraviolet to TiO_2. Their analysis did not attempt to include the possible effects of nonspherical particles, as only phase angles between 20 and 90° could be observed. Pollack *et al.* (1977) identified magnetite as the opaque mineral phase at visible wavelengths and, since magnetite also has an absorption maximum in the ultraviolet, suggested that it is responsible for the feature described by Pang and Ajello (1977). Apparently, no detailed comparison with the Mariner 9 UVS data has been carried out. Given the phase function observed by the UVS, a study which included nonspherical effects and tested magnetite as a candidate for the ultraviolet absorption feature might provide additional information about the particle size distribution during the 1971b storm and an interesting test of the semiempirical parameterization used to include the effects of nonspherical particles in the modeling of the Viking Lander sky brightness data. According to Pollack *et al.* (1979), only 1% of each particle's volume need be magnetite in order to produce the optical parameters required at visible wavelengths.

At infrared wavelengths, Mariner 9 IRIS observations revealed broad spectral features near 10 and 20 μm, which indicated the airborne dust was highly silicic (Hanel *et al.*, 1972). Toon *et al.* (1977) compared Mariner 9 IRIS observations to theoretical spectra generated with a two-stream radiative transfer model based on a three-parameter particle size distribution, the temperature profile retrieved from the IRIS CO_2 band spectra, and the optical constants of several candidate dust analogs. Mie scattering models were used to generate $\tilde{\omega}_0$, g, and Q_{EXT} as a function of wavelength. The best fits were obtained for $\bar{r}$ = 2.5 μm and for montmorillonite 219b. (Note that for particles of this size the effects of nonspherical shape can be neglected at infrared wavelengths, so the Mie scattering calculations were appropriate.) Given that the dust is probably a complex combination of different materials, the above fit to the IRIS spectra is not unique, but whatever the composition of the airborne dust is, it must yield optical parameters ($\tilde{\omega}_0$, g, and τ) similar to those derived by Toon *et al.* (1977) with their size distribution and the montmorillonite 219b complex refractive index, since it is these optical parameters which are most directly tested by the comparison of the theoretical and observed spectra. In this regard, Toon *et al.* (1977) found that mixtures of montmorillonite and basalt gave a somewhat better fit to the Mariner 9 IRIS data in the 20-μm region. Hunt's (1979) parametric studies of an isothermal dust cloud suggested that a mixture of basalt and montmorillonite, rather than montmorillonite alone, was also required to explain certain of the Viking IRTM 20-μm-channel data.

TABLE I

MARTIAN GREAT DUST STORMS

Year	Citation	L_S[4]	Initial location
1909 (Aug)	*2, 3*	—	—
1911 (Nov)	*2, 3*	—	—
1922	*1, 2*	192	—
1924 (Oct)	*3*	—	—
1924 (Dec)	*1, 2, 3*	237	Isidis Planitia
1939[5]	*2, 3*	—	Utopia?
1941[5] (Nov)	*3*	—	South of Isidis
1943	*1*	310	Isidis
1956	*1, 2, 3*	250	Hellespontus
1958	*1, 3*	310	Isidis
1971 (July)	*1*	213	Hellespontus
1971 (September)	*1, 3,* Mariner 9	260	Hellespontus
1973	*1*	300	Solis Planum, Hellespontus
1977 (February)	Viking	205	Thaumasia Fossae
1977 (June)	Viking	275	—
1979	Viking	225?	—

[1] Briggs *et al.* (1979).
[2] Capen (1971).
[3] Michaux and Newburn (1972). This reference also cites several "major" dust storms identified only on Lowell Observatory photographic plates and not referenced elsewhere. These events (October, 1909; September, 1911; 1926; August, 1941) are not listed above.
[4] Seasonal date of the regional onset of the great dust storms (Briggs *et al.*, 1979; Ryan and Henry, 1979; Ryan and Sharman, 1981).
[5] These clouds may have remained localized phenomena.

DUST STORM FREQUENCY

"Ocher-colored veils" obscuring parts of the Martian disk were reported as long ago as 1800 by H. Flaugergues. Since that time, planetary-scale obscurations of Mars have been seen from the Earth during each of the most favorable (perihelic) oppositions (1909, 1924, 1939, 1956, 1971) and often during other, somewhat less favorable, oppositions (see Table I). Although local dust storms—the yellow clouds of Mars—have been observed on Mars during all seasons (Gifford, 1964; Capen, 1974; Briggs and Leovy, 1974; Peterfreund and Kieffer, 1979), the great dust storms have not been observed to originate during northern spring or summer, when Mars is farthest from the Sun and also most difficult to view from Earth.

Figure 1 shows the seasonal date of those Martian great dust storms whose regional onset was observed from Earth and/or by spacecraft (Briggs *et al.*, 1979) or by the Viking Lander. When more than one storm has occurred in a single (Earth) year, they are designated a or b (as in 1977a) in the order of their appearance. Identifying a dust storm as "great" implies that it covered a large area of planetary, but not necessarily global, scale. Given the selectivity of the historical record due to the ever-changing distance between Earth and Mars, the observational record suggests that one, or occasionally two, dust storm of planetary scale may occur each Martian year. The duration and extent of these storms vary greatly, however. Those storms which occur in early southern spring (e.g., 1971a, 1977a, 1979), long before perihelic passage (at $L_S = 250°$), tend to cover smaller areas and to be shorter lived than the great dust storms which occur at or after perihelion. Lander observations of the two 1977 great dust storms suggest that the maximum atmospheric opacity occurring during these smaller events is less than that which occurs in the larger, longer-lived great storms. The more expansive perihelic storm may follow an earlier, smaller precursor storm, as happened in 1977 during the Viking Mission and in 1971 when Mariner 9 arrived at Mars. The 1971b storm was perhaps the largest and most truly global of the Martian dust storms yet observed. No storm similar to the 1977b storm appears to have occurred during 1979, the second Martian year of Viking observations, even though the Lander meteorological data indicated that in 1979 a somewhat smaller storm occurred at almost the same seasonal date as the 1977a event (Leovy, 1981; Ryan and Sharman, 1981).

DUST STORM EVOLUTION

Perhaps the most fundamental questions concerning the great dust storms on Mars are related to their origin. Recent Earth-based and spacecraft observations of Mars have not significantly changed the classical view summarized by Gierasch (1974) of the onset of a great dust storm. In this view one or more regional dust storms develop during southern summer or spring in one of three preferred locations: (1) the sloping plains between the northwest rim of Hellas and the Noachis uplands, where both the 1956 and 1971 great dust storms originated, (2) the sloping plains to the west, south, and southeast of Claritas Fossae, where the main centers of the 1973 and 1977a storms developed, and (3) the low-lying Isidis Planitia to the east of Syrtis Major (see Table I). These local dust clouds expand slowly during an initial phase lasting, typically, 4 days. Expansion becomes more rapid during the next 4 days, new centers of activity develop, and old ones coalesce. At first, expansion occurs largely in an east–west direction, and after an additional 5–10 days, the dust haze has encircled the planet. Many of the core regions established during the early phases remain active and distinguishable during the later stages of the great storm. Once the great dust storm enters its decay phase, the planetary-scale dust haze slowly dissipates over a period of several weeks.

Any model attempting to explain the origin of the great dust storms must address at least three critical questions: (1) why do these precursor storms originate only in certain areas during certain seasons, (2) by what mechanism do some, but certainly not all, local storms evolve to planetary scale, and (3) how widespread is the source of the dust that eventually winds up in the planetary-scale dust haze? A fourth question which has important climatic implications asks where the dust raised by a great storm is deposited.

The most complete coverage of the onset stage has been provided by Earth-based observations, particularly the cloud maps derived from the photographic images obtained by the International Planetary Patrol (Baum, 1973) of the 1971b and 1973 great dust storms (Martin, 1974, 1976). These observations show that great dust storms evolve from much more localized storms, yet most local dust storms do not evolve into planetary-scale disturbances. Thus, the local dust storm appears to be a necessary, but not sufficient, predecessor to the great storm. Historically, local "yellow" clouds have been observed to occur most frequently in the approximate latitude belts 10–20°N and 20–40°S, with more clouds seen in the south than in the north and with more frequent sightings during southern spring and summer (Michaux and Newburn, 1972). Thus local storms are apparently most likely to occur during the same periods and in the same areas as the great dust storms.

After the 1971b storm subsided, Mariner

9 observed local storms near the edge of the north polar hood and in Chryse Planitia (Leovy *et al.*, 1972; Briggs and Leovy, 1974). Viking saw local storms primarily in the southern hemisphere during southern spring and summer, although this latitudinal asymmetry may be due to the lack of comparable coverage in the north at this time. The local dust storms which Viking detected in the southern hemisphere either by imaging at visible wavelengths or by mapping the IRTM radiances (Briggs *et al.*, 1979; Peterfreund and Kieffer, 1979) can be divided into two groups: those occuring within 10–15° of latitude of the receding south polar cap[4] and those in the 10–30°S latitudinal zone. The first group is easily explained as the result of strong winds driven by the mass outflow and the large temperature gradient at the edge of the subliming cap (Leovy *et al.* 1973; French and Gierasch, 1979; Haberle *et al.*, 1979), and also by traveling waves (eddies or weather systems) generated in the baroclinic zone equatorward of the polar cap edge (Leovy, 1981; Ryan and Sharman, 1981). Almost all of the subtropical group of local dust storms occurred in the Claritas Fossae/Solis Planum area. No local storm was observed by Viking in Hellespontus/Noachis or Isidis, the other two regions where both local and great dust storms are most likely to occur. Both of the 1977 great dust storms observed by the Viking orbiters are thought to have originated in the Thaumasia Fossae/Solis Planum area. Thus interannual variability in local dust storm activity may determine which of the three regions will spawn a great dust storm in any given year. Each of the three regions is associated with major topographic relief (particularly east- or southeast-facing slopes) and with major boundaries in surficial properties, such as albedo and/or thermal inertia (Peterfreund and Kieffer, 1979; Peterfreund, 1981). Uplands can act as elevated heat sources (Blumsack *et al.*, 1973; Zurek, 1976; Webster, 1977), and airflow over and around orography can enhance local convection (French *et al.*, 1981) as well as the dynamic forcing of the large-scale circulation (Gierasch and Sagan, 1971; Mass and Sagan, 1976; Webster, 1977; Moriyama and Iwashima, 1980; Pollack *et al.*, 1981). Because atmospheric temperatures in a relatively clear, thin CO_2 Martian atmosphere are so strongly influenced by heat radiated or convected from the surface, gradients in surficial albedo and thermal inertia should also be important in producing winds (Blumsack *et al.*, 1973; Peterfreund and Kieffer, 1979), particularly on local spatial and diurnal time scales. On planetary scales the general diurnal variation of surface heating during relatively clear periods and of solar heating of the airborne dust during dusty periods drives large-amplitude atmospheric tides, and these large-scale tidal winds have their near-surface maximum speeds 20° of latitude away from the equator. The nearly symmetric (in latitude) tidal wind maxima are consistent with the historically observed tendency for local dust storms to occur in the subtropics of both hemispheres, while the combination of the planetary-scale circulation, including tides, and of topographically induced winds may account for the observed longitudinal sectors where local—and great—dust storms are most likely to occur.

For a dust storm of any size to develop, dust must be raised into the atmosphere. This requires a source of movable dust, as well as surface winds strong enough to move it. Even the particles most likely to be moved on Mars require substantial near-surface winds (Sagan and Pollack, 1969; Greeley *et al.*, 1980). Winds exceeding 25 m sec^{-1} were observed (Ryan *et al.*, 1981) by the Viking Lander 1 meteorological instruments 1.6 m above the surface during the only local dust storm observed at the Lander sites (James and Evans, 1981). Since dust must have been raised locally at this time, these winds probably were strong

[4] These storms are in mid-latitudes (30–60°S) prior to the onset of the 1977a great dust storm at $L_S \sim 208°$.

enough to raise dust. This is consistent with estimates of the saltation threshold and with other Lander evidence of particle movement on the surface of Mars during peak winds (Sagan *et al.*, 1977). Winds exceeding 25 m sec^{-1} were rarely seen at the Lander sites, however, and they were more likely to occur at the more northern site (VL2) due to the traveling baroclinic waves which were present during northern fall and winter (Barnes, 1980; Ryan and Sharman, 1981). Thus a favorable combination of different wind regimes appears to be required to exceed the threshold for moving dust from the surface. Since these regimes have different characteristic temporal and spatial scales, it is perhaps not surprising that this favorable combination—and the local dust storm it generates—usually lasts only a few days.

The necessity for the favorable superposition of various wind regimes is also suggested by the concentration of the so-called dark streaks, which are low-albedo ragged streaks lying behind topographic relief features, in Syrtis Major and in latitudes 20–40°S (Thomas *et al.*, 1981). These are virtually the same regions where dust storms are most likely to occur. The dark streaks are believed to be erosional areas where thin deposits of relatively brighter material are removed in the turbulent wakes behind craters, scarps, and occasionally troughs (Sagan *et al.*, 1972; Thomas *et al.*, 1981). Most of these dark streaks disappear during great dust storms, after which they are soon regenerated. High winds are needed to entrain the brighter, smaller ($\sim$2 μm) dust particles deposited from the general dust haze of a great dust storm, and this is consistent with the association of dark streaks with particular topographic features (Veverka *et al.*, 1981). On the other hand, the correlation (Peterfreund, 1981) of the dark streaks with areas which may have average particle sizes $\gtrsim$80 μm, as determined from the IRTM observations of diurnally varying surface temperatures, suggests that the areas where dark streaks and dust storms tend to occur may have relatively more of the most easily moved particles.

Great dust storms tend to develop not only in certain preferred areas, but also during certain seasons, namely, southern spring and summer, although one must again recall the uneven coverage provided by both Earth-based and spacecraft observations. The most reliably observed regional onsets of Martian great dust storms (Fig. 1) all occur within 60° of L_S of perihelion passage at $L_S \sim 250°$, which is near southern summer solstice at the current epoch. During this period the available insolation is 94–100% of the maximum available, and the subsolar point is between 8 and 25° south of the equator. During relatively clear periods the increased surface heating in this latitudinal zone and at this time will certainly enhance atmospheric convection during the day and will strengthen winds induced by the thermal effects of topography. The cross-equatorial (Hadley) branch of the axially symmetric circulation will also intensify and expand near summer solstice (Leovy and Mintz, 1969). However, the planetary-scale atmospheric tides change little, since most of the latitudinally antisymmetric tidal heating drives a mode which produces little surface pressure variation (Zurek, 1976).

Given that these local dust storms occur when and where they do, how—and why—does the planetary dust storm evolve? Mechanisms for generating a great dust storm have traditionally been divided into two classes (Gierasch, 1974), one of which emphasizes planetary-scale components of the atmospheric circulation (Leovy *et al.*, 1973; Houben, 1982) and the other the organization of small but expanding scale vertical motion through a strong dust feedback (Hess, 1973; Golitsyn, 1973; Gierasch and Goody, 1973). Both types of model depend on the diabatic heating due to the absorption of solar radiation by airborne dust to sustain the dust storm's growth, but they differ most radically concerning the horizontal scale of the *initial* diabatic forcing.

Gierasch and Goody (1973) showed that if a local dusty core region developed in the presence of a weak cyclonic flow, as might occur above an elevated plateau, then solar heating of the dusty core would intensify the horizontal gradients of temperatures at the core's periphery and, through Coriolis torques, accelerate the cyclonic flow spiraling inward into the dusty core. The greater velocity and expanded reach of the spiraling flow generated by this vorticity convergence would raise and entrain dust in the planetary boundary layer feeding the dusty core, increasing the opacity of the core and thus intensifying the storm's development. In this model, which is analogous to models of terrestrial hurricanes except for the depth of the storm and the use of dust rather than latent heating, the early stages of the storm are characterized by swirling motions. In general, the local dust storms observed by Viking (Briggs *et al.*, 1979) do *not* exhibit such motions. The simplest explanation of this is that the winds on Mars are typically too strong in the regions where great dust storms originate to permit the organization of the initial, small-scale cyclonic swirl. The only spiral clouds observed on Mars appeared at high northern latitudes in (northern) summer at a time and place where winds were thought to be very weak (Gierasch *et al.*, 1979).

The other class of models (Leovy *et al.*, 1973; Pollack *et al.*, 1979; Leovy, 1981) emphasizes the enhancement of the planetary-scale circulations in the following manner: local dust storms develop during southern spring in the baroclinic zone in the southern mid-latitudes adjacent to the retreating south polar cap. These dust storms result from the strong surface winds at the cap's edge (Leovy *et al.*, 1973; Haberle *et al.*, 1979), from the weather systems developing in the baroclinic zone, and/or from mountain lee waves (e.g., in Argyre) in the belt of strong westerlies above the baroclinic zone. The dust raised by these storms is carried equatorward and thus raises the dust loading over the Martian low latitudes. Even optically thin dust hazes can produce significant solar heating rates (Gierasch and Goody, 1972; Moriyama, 1975; Zurek, 1978; Pollack *et al.*, 1979). This augmented diabatic forcing intensifies the general circulation (including atmospheric tides), particularly over the sloping terrain of the 20–40°S zone (Webster, 1977; Zurek, 1976; Conrath, 1976). Within this zone, it is through topographic control that planetary-scale, regional, and local winds combine to raise dust in the preferred locations near Tharsis and Hellas. Thus, the enhanced planetary-scale circulation provides the necessary background wind, so that local mechanisms such as slope winds, turbulent wakes, boundary layer instabilities (Brown, 1974), or convective intensification over sloping terrain (French *et al.*, 1981) can maintain for many days the local dust storms which form the core areas of the developing great storms. These areas are hardly in a steady-state equilibrium, but they do persist, even if their sometimes daily regeneration (Martin, 1974, 1976) really consists of the dissipation of one local storm followed by the generation of another. This persistence would be largely due to the background wind provided by the enhanced planetary-scale circulation. As dust spreads from these core areas, it tends to parallel terrain contours even as it spreads in a generally east–west direction (Martin, 1974, 1976; Briggs *et al.*, 1979); this would reflect the topographic modulation of the planetary-scale circulation (Webster, 1977; Moriyama and Iwashima, 1980). The solar heating of the optically thick core areas must be intense, as it is in all local dust storms, and this is reflected in their morphology as viewed from above: parallel striations in a turbulent mass, with lobate or turret-like structures suggesting convection along their most sharply defined edge (Briggs *et al.*, 1979; James and Evans, 1981). As the southern subtropics where the core regions reside become progressively dustier, the resulting zonal solar heating will correspondingly intensify the thermally direct, upper-level northward flow. Since upper-level winds are generally stronger than the near-surface flows, the dust will spread more quickly as it is carried upward in the ascending branch of the intensified, cross-equatorial solstitial circulation (Leovy *et al.*, 1973; Haberle *et al.*, 1982). The enhanced planetary-scale circulation, together with more local winds driven by the differential solar heating, will raise dust in new areas where surface winds were not previously strong enough to raise dust.

As seen from the Viking Landers, the 1977 great dust storms were marked by an enormous increase in the overhead dust opacity. This increase occurred in only 1 or 2 days (Pollack *et al.*, 1979) and, although the opacity histories are less certain during the period when $\tau > 2.5$, this increase was apparently followed in, at most, a few days by an exponential decline in the opacity of the dust haze (Fig. 2). This sudden increase and almost immediate decline are most easily explained as the advection over the Lander sites of a dust haze which is already thinning. Unfortunately, there is no direct information about the vertical distribution or optical properties of the dust at this time, and inferences based on the Lander meteorological data are somewhat ambiguous (Zurek, 1981). It is not known whether this dust comes from the region of onset or from more local sources in the northern hemisphere. There appears to have been little movement of surface dust at the Viking Lander sites during the 1977 storms (Sagan *et al.*, 1977), which is consistent with the Lander wind data (Ryan and Sharman, 1981). Earth-based observations of the 1971b and 1973 great dust storms (Martin, 1974, 1976) suggest that 10 m sec^{-1} is a typical north–south velocity during the expansion of a great dust storm. This is similar to Thorpe's (1979, 1981) estimates based on the Viking Orbiter imaging data for the 1977a storm and somewhat higher than his estimates for the 1977b storm. The nearly simultaneous arrival of the optically thick dust hazes above the Viking Landers (Pollack *et al.*, 1979; Ryan and Henry, 1979) implied faster rates of expansion for both 1977 storms, but this interpretation assumes that the expansion is zonally symmetric, since the Landers are 180° of longitude, as well as 25° of latitude, apart. Observations show that longitudinal variations do occur (Martin, 1974; Thorpe, 1982). Local dust storms have been observed to move with somewhat higher velocities of 15 to 50 m sec^{-1} (Peterfreund and Kieffer, 1979; James and Evans, 1981). Thus the observed expansion velocities of the great dust storms are more consistent with the transport, rather than the raising, of dust.

On the other hand, Pollack *et al.* (1979) calculated that if dust was injected only by local storms or core areas covering 1% of the planet's total area, then these source regions were losing ~1.5 mm of soil per terrestrial year. If sustained over a precessional cycle (~10^6 years), more than a kilometer of surface would be lost in the source regions, assuming no recycling of the dust. The main and secondary core regions observed from Earth during the 1971b dust storm covered perhaps 10% of the planet (Martin, 1974, Fig. 8); this area is an order of magnitude larger than that used in the calculation by Pollack *et al.* (1979). Although a core area of a great dust storm may begin as a local dust storm covering perhaps 10^5 km^2, it expands and coalesces with new centers to cover much larger areas in only a few days. By the time a great dust storm enters its mature stage, when it encircles the planet and expands into the northern hemisphere, much of the zone between 10 and 50° may be a source region.

Not all great dust storms do expand into the northern subtropics (Capen and Martin, 1971). The ability of these storms to expand significantly northward may well depend on how high the dust is carried over the source region. This in turn may depend upon the background dust loading and the static stability of the middle atmosphere. Using a zonally symmetric circulation model, Haberle *et al.* (1982) found that dust is raised up to 20 km or more before significant northward transport occurs. Observations of the atmospheric temperature in a broad layer centered at 25 km by the Viking IRTM showed that dust was carried to at least these altitudes during the 1977 storms (Martin and Kieffer, 1979; Leovy and Zurek, 1979). During the truly global 1971b storm, Mariner 9 television images of the limb of Mars indicated that dust was mixed at up to 40–60 km of altitude (Leovy *et al.*, 1972). The high-altitude temperatures observed by the Mariner 9 IRIS also indicated that dust was present at 40 km altitude (Conrath *et al.*, 1973).

Once the dust storm has obscured most of one hemisphere and perhaps much of another, the atmosphere begins to clear. This decay phase is generally attributed to the increasing static stability above the regions where dust is raised (Pollack *et al.*, 1979; Leovy and Zurek, 1979). This increased static stability should effectively suppress boundary layer turbulence and/or decouple the near-surface winds from those aloft. Observations (Conrath *et al.*, 1973; Lindal *et al.*, 1979; Martin and Kieffer, 1979) clearly show that the Martian atmosphere is certainly more isothermal and thus stable during the decay phase. Even if local storms were still active, the greatly enhanced stability would limit the ability of such storms to convectively raise dust high into the atmosphere where it could most easily spread. Opacities greater than one will also suppress surface heating (Pollack *et al.*, 1979) and its associated diurnal temperature variation and convection. The time constant estimated for the decay phase was 60 sols for the 1971b storm (Conrath, 1975), 75 sols for the 1977a storm, and 51 sols for the 1977b event (Pollack *et al.*, 1979). This tendency for great dust storms which occur later in northern fall and winter (see Fig. 1) to have shorter decay times may be due to scavenging of the dust by ice condensation and gravitational sedimentation over the growing seasonal north polar cap. An extended analysis (Anderson and Leovy, 1978) of the Mariner 9 television images of the Martian limb showed a decay rate of the 1971b haze over low latitudes which was consistent with Conrath's (1975) estimate based on the decreasing diurnal temperature variation observed by the Mariner 9 IRIS at different altitudes above the zone 20 to 30°S. However, Anderson and Leovy (1978) also found a more rapid clearing of high latitudes. These observations were consistent with scavenging of the dust by ice over the polar caps (Pollack *et al.*, 1979) and/or with enhanced vertical mixing of the airborne dust above the tropics by vertically propagating atmospheric tides (Zurek, 1976). It should be remembered that the inference that the size of the particles remained essentially unchanged during the decay phase of the 1971b storm was based largely on low-latitude observations (Conrath, 1975; Toon *et al.*, 1977). Outside the tropics, atmospheric tides will be less effective in mixing the atmosphere. The atmospheric static stability will be large over the CO_2 polar ice, so that gravitational settling could remove airborne dust to the surface even without the particles serving as condensation nuclei. Of course, condensation of water or carbon dioxide on the dust particles will make the gravitational settling more rapid and efficient. This particular sink of airborne dust is tremendously important climatologically, since the deposition of a dust–ice mixture onto the polar cap over great periods of time (10^5 years or more) may have led to the polar laminated terrain (Pollack *et al.*, 1979). The amount of material available for deposition depends on how much material enters the polar atmosphere. Unfortunately, we do not yet understand how dust is transported over the polar caps. The expanded zonally symmetric circulation associated with the great dust storm probably does not extend beyond the region of large temperature gradient adjacent to the condensing cap. This is consistent with the numerical modeling of the zonally symmetric circulation by Haberle *et al.* (1982) and with the high-pressure regime observed at Lander 2 during the 1977b storm. However, the general increase in temperature near 25 km of altitude observed during the 1977b storm was particularly large in the polar night (Martin and Kieffer, 1979), so that heat must have been transported into the atmosphere above the condensing polar cap. This is also suggested by Earth-based observations which show a diminution of the north polar hood (ice haze) during the decay phases of a great dust storm (Martin, 1975). Ryan and Henry (1979) found a correlation between northward wind and increased opacity at the Lander 2 site during the period between the two 1977 great dust storms, implying that the weather systems observed at this northern site (Ryan and Henry, 1979; Barnes, 1980, 1981; Ryan and Sharman, 1981) can transport dust as well as heat into the interior of the polar cap. These weather systems were not as evident during the 1977b storm itself, but the expanding zonally symmetric circulation may have simply pushed the baroclinic zone where the traveling waves originate farther to the north. Dust may not have to be immediately transported over the polar cap during a great dust storm in order for it to end up there. Local dust storms or baroclinic waves associated with the polar cap retreat during spring and summer or with the traveling storm systems during fall and winter may also inject dust into the polar regions. This dust could have been transported from lower latitudes during the last great dust storm, yet deposited at that time outside the polar cap, perhaps in the zone of the subsiding branch of the axially symmetric circulation. During the period of polar cap retreat, the local storms will have to work against the low-level (sublimation) mass outflow, but some dust might be injected if dust is raised high enough or if the polar outflow varies greatly with longitude. The entrainment of substantial dust into the north polar cap might account for the noticeably lower albedo of the north cap as compared with the south (D. Paige, private communication). High southern latitudes were observed to remain relatively clear during the 1977a storm even though local storms did occur near the periphery of the polar cap. The entire south polar region was at least partially obscured during the 1956, 1971, and 1977b great dust storms. Atmospheric dust over or near the ice caps may either enhance or reduce the rate of sublimation of the retreating cap depending upon the effective albedos of the ice surface and of the dust haze (Davies, 1979). The Viking data showed that the 1977 retreat of the south polar cap was slower than the historically observed retreat, and this anomaly has been attributed to the early 1977a great dust storm (James *et al.*, 1979). More accurate estimates of the optical parameters of the surface and dust haze are needed to confirm this hypothesis and to determine whether or not the great dust storms can significantly alter the size of the residual reservoirs. One would like to know, for instance, if the south residual cap could lose all of its CO_2 cover, as did the north residual cap observed by Viking (Kieffer, 1979), and whether or not interannual variation in the polar caps reflects changes in the atmospheric dust.

Away from the condensing polar caps dust is removed from the atmosphere by vertical mixing onto the surface. The rapid reemergence of surface albedo features following a great dust storm, and the fact that the classical albedo features on Mars have persisted for 200 years or more, indicates a remarkable degree of efficiency and regularity in the processes which remove dust locally to form the persistent patterns of both large and small albedo-features (Peterfreund, 1981; Christensen, 1982). The obliteration of dark streaks during a great dust storm and the widespread formation of bright streaks during its decay (Thomas *et al.*, 1981) demonstrate that dust deposition from a great storm is as widespread as the haze itself. A likely mechanism for forming the bright streaks requires high static stability during dust-storm decay to produce quiescent areas of deposition downwind of crater rims (Veverka *et al.*, 1981). As noted above, the decay of the great storm may be due to this same stability. As the opacity of the dust haze declines, surface heating will become more important, and the atmosphere will become less stable. Turbulent wakes behind obstacles may then erode some of the recently deposited dust to form the dark streaks (Veverka *et al.*, 1981). The Viking IRTM data suggest that the dust fallout from a great storm is preferentially removed from low-albedo, high-thermal inertia areas in the Martian low latitudes (e.g., Syrtis Major) and that this dust may then be redeposited at higher northern latitudes (Christensen, 1982). As the surface dust is reworked, the classical albedo features reappear. Pollack *et al.* (1979) have suggested that the slower decay rate observed at Viking Lander 1 during the later decay phase was due to the resurgence of local dust storms when the opacity declined to $\tau \sim 1.25$. Local dust storms were observed by orbiting spacecraft during the 1971b and 1977a great dust storms, but not during the 1977b storm (Leovy *et al.*, 1972; Peterfreund and Kieffer, 1979; Briggs *et al.*, 1979). Although observational coverage was not complete, a more comprehensive search of the Viking IRTM data for local storms in 1977 might better define the activity of local dust storms. The reduced static stability of an atmosphere characterized by $\tau \sim 1$ may also permit more general dust raising as represented by the reformation of the dark streaks. These mesoscale processes, augmented by occasional local storms, may account for the background opacity of $\tau \sim 0.4$ observed when Viking first landed on Mars.

Pollack *et al.* (1979) have noted that the opacity was near unity at Viking Lander 1 prior to the onset of both 1977 great storms. The planetary-scale circulations will continue to intensify for $\tau > 1$, but local winds, such as turbulent flow over a crater or scarp, appear to be suppressed by the high static stability associated with $\tau > 1$. Thus $\tau \sim 1$ may well be the optimum opacity of the widespread dust haze with regard to the positive feedback which generates a great dust storm. If this is so, why are not all of the early (preperihelion) great dust storms followed by a second dust storm as happened in 1977, but not in 1979? Leovy (1981) has suggested that the seasonal south polar cap retreat and its associated (midlatitude) local dust storms lead almost yearly to a great dust storm in early southern spring through the interaction between planetary-scale and local wind systems, as apparently happened in both Mars years of Viking observations. The postperihelic storms, on the other hand, develop only if the somewhat special, almost random, conditions required to generate amplifying planetary-scale atmospheric tides occur during the decay of the year's first great dust storm. Thus the 1977b storm was observed to develop immediately after a period of unusual tidal activity (Leovy, 1981), while no such activity or storm was observed following the preperihelic 1979 storm. If it occurs, the year's second great dust storm would be more extensive and long lived than the first, as it was in 1971 and 1977, because of the more widespread dust and, perhaps secondarily, because the second storm would originate near the time of maximum insolation.

Zurek and Leovy (1981) showed that a thermally forced diurnal Kelvin tidal mode could account for the unusual activity observed at Lander 1 prior to the 1977b storm. Conrath (1976) detected the presence of a similar tidal mode during the decay phase of the 1971b storm. This eastward-traveling tide would be directly forced by the solar heating of a low-latitude dust haze whose longitudinal distribution was primarily wavenumber 2. Enhanced dustiness over the Tharisis/Solis Planum and Syrtis Major/Isidis sectors might provide the required forcing. Houben (1982) has proposed that the onset of a great dust storm is triggered by an unstable (i.e., characterized initially by exponential growth) tidal mode similar to the diurnal Kelvin mode described above. The explosive growth of this mode results from the advection of the dust by the planetary-scale wave in such a way that the dust perturbation reinforces the diabatic forcing of this particular wave. Thus Houben (1982) suggests that the unstable mode generates the special dust configuration needed for its growth, while Zurek and Leovy (1981) assume that a similar configuration exists due to other mechanisms. As presently derived, both tidal mechanisms presuppose the existence of a widespread, moderately thick dust haze. As such, they are more likely candidates for triggering the second of two dust storms, rather than the first. They even contain their own switch-off mechanism independent of the role of static stability: dust raised by the tidal winds drives other planetary-scale winds which destroy the special distributions of dust which enhance these particular modes.

One may still ask why great dust storms do not occur during the corresponding northern seasons. (Note that great dust storms have apparently originated in the northern hemisphere, in Isidis (see Table I), but that they occurred in northern winter.) Certainly there is an intense baroclinic zone adjacent to the north polar cap edge where local dust storms are known to develop (Briggs and Leovy, 1974; Leovy *et al.*, 1972). However, because of the ellipticity of the orbit of Mars and the present occurrence of aphelion in late northern spring, the insolation available at $L_S \sim 20°$ is only 74% of that available at $L_S \sim 200°$ during the present epoch. This reduces the intensity of the planetary-scale circulations and the likelihood of local convective activity; either effect may be sufficient to suppress the development of great dust storms. If or when great dust storms occur in the north, they may well originate in the Lunae Planum/Chryse or Syrtis Major/Isidis areas, since these regions appear to have the large gradients in surface height and surficial thermal properties at low latitudes (Palluconi and Kieffer, 1981) needed to produce high winds. These regions may also have an ample source of the most easily moved material. However, the topography of the northern hemisphere is sufficiently different from the southern that the possibility exists that great dust storms may be smaller or may occur less frequently, if at all, even during epochs when the maximum insolation occurs near northern summer solstice. This may result from the inability of the various wind components to reinforce one another properly, or from the inability to move the dust raised by storms near the north polar cap's edge onto the generally higher ground of the Martian low and cross-equatorial latitudes. General availability of saltating particles in the region of highest winds may also be a factor. An asymmetry in the frequency of great dust-storm occurrence could be one factor responsible for the possibly large difference in the extent and volume of material contained in the north, as opposed to the south, polar laminated terrain.

CONCLUSIONS

In summary, the most direct—and probably reliable—estimates of opacity are those derived from Viking Lander imaging of the Sun. Furthermore, the opacity above Viking Lander 1 is fairly representative during great dust storms of the widespread dust haze covering the Martian low latitudes, although local variations ranging from local dust storms to nearly haze-free areas do occur. Opacities estimated from the Lander meteorological data, from the Viking Orbiter infrared remote sensors, and from Orbiter visual imaging can substantially augment the Lander imaging opacity histories. Because these estimates are highly model dependent and require the input of several—often poorly known—parameters, they must be used with caution and be intercompared among themselves and against the opacities derived from Lander imaging whenever possible. Discrepancies between various estimates need to be understood, not only to improve the estimates themselves, but also to understand more fully the effects of parametric values and simplifying assumptions commonly introduced in the theoretical modeling of the thermal forcing of the Martian circulation and climate. In these respects, the potential of those methods which use Viking Orbiter data to determine opacities across the globe and/or at the Lander sites during the dustier ($\tau \gtrsim 2$) periods has not yet been fully exploited. As for the Lander data, the continued operation of the Lander 1 imaging and meteorological systems may extend the present opacity history to 1994, albeit with less temporal resolution.

The radiative properties of the airborne dust are characterized at visible wavelengths by $\tilde{\omega}_0 \sim 0.85$, $g \sim 0.5$–0.8. Magnetite appears to dominate the visible optical properties. At infrared wavelengths, the complex refractive index of montmorillonite 219b and the particle size distribution derived by Toon *et al.* (1977) yield optical parameters which are consistent with the Mariner 9 IRIS observations, although there is some evidence that basalt mixed with montmorillonite yields a better fit in the 20-μm wavelength region. These optical properties must be used with some caution. All are model dependent. Unlike the case for τ, this is as true for those parameters estimated from the Lander imaging data as for those estimated from Orbiter observed radiances. Pollack *et al.* (1979, p. 2934) provide an illustrative example of a nonunique fit to a large subset of the Lander imaging data, and one can perhaps take the resulting changes in optical parameters ($\bar{r} = 0.4$ to $2.5\ \mu$m, $\tilde{\omega}_0 = 0.75$ to 0.86, and $g = 0.6$ to 0.79) as representative of the modeling uncertainties. It may also be too much to expect that dust raised at different times, in different places, or by different wind regimes is always of the same size or composition. This may be particularly true for local dust storms, even though there is some evidence that the widespread dust hazes extending high into the atmosphere may be more uniform.

Great dust storms on Mars appear to evolve from local storms in preferred regions where a favorable combination of the seasonal planetary-scale circulation, atmospheric tides, and regional and local topographically induced winds can raise dust more or less continuously for several days. These regions—Claritas Fossae/Solis Planum, Hellespontus/Noachis, Syrtis Major/Isidis—are characterized by their location in low and subtropical latitudes, by the presence of large east-facing slopes, by strong gradients in surficial albedo or thermal inertia, and perhaps by regional sources of the most easily moved (saltating) surface material. The great dust storms occur during the period of maximum insolation (southern spring and summer, $L_S \sim 190$ to $310°$), but onset still may require augmentation of the planetary-scale circulation by solar heating of a moderately thick ($\tau \gtrsim 1$), widespread dust haze provided by local dust storms generated in the mid-latitude, baroclinic zone adjacent to the retreating south polar cap.

Superimposed on this enhanced general circulation (including tides), local slope winds and boundary layer convective instabilities can produce one or more extensive core regions in the southern subtropics where dust is raised into the atmosphere and is then rapidly distributed longitudinally. The solar heating of this dusty corridor drives a greatly intensified zonally symmetric circulation which transports dust northward even as it raises dust in new areas as it expands. The extent of this expansion appears to be limited by the opacity and vertical distribution of the low-latitude dust haze, since the intensity and (dynamic) stability of the zonally symmetric circulation is directly related to both the solar heating and the associated increase in the static stability. The increased stratification of the vertically extended dust haze will also suppress or decouple near-surface winds and thus initiate the decay phase of the storm. A second great dust storm may follow the first if the decay of the first storm leaves a dust distribution, perhaps controlled by topography, whose heating drives resurgent atmospheric tidal modes. Storms occurring near or after perihelion apparently cover greater areas, perhaps because of more insolation or of a more widespread prestorm haze. Great dust storms do not occur in northern spring and summer because of the greatly reduced insolation available at that time during the present epoch. However, because of the radically different topographies—both in height and surficial properties—of the northern and southern hemispheres, northern great dust storms may happen less frequently than their present-day southern counterparts, even when perihelion occurs near northern summer solstice. Some of the dust raised in a great dust storm may be scavenged by condensation of water and CO_2 into the condensing seasonal polar cap. Dust deposited at high mid-latitudes may also eventually be transported into the polar regions by local dust storms. The polar laminae and possible differences in the overall volumes of north and south-polar laminated terrains may reflect very long-term variability in the frequency of great dust storms and their ability to inject large amounts of dust into high latitudes.

The above outline of dust-storm evolution contains several critical, but only vaguely—at best, qualitatively—defined mechanisms. Major points to be clarified are the determination of what horizontal and vertical distributions of atmospheric dust will permit a local dust storm to grow to planetary scale and what sources of dust will contribute to the great dust storm once it has expanded to cover much of Mars. Present estimates of the optical parameters and the vertical distribution of the atmospheric dust are based on measurements made long before the onset of a great dust storm or during its decay phase; these properties need not be the same during the onset phase. Ongoing studies of the Viking data may be expected to provide additional clues. Data from the continuing operation of Lander 1 will be particularly valuable. Otherwise, interdisciplinary studies utilizing several different data bases perhaps hold the greatest potential for data analysis. An equally exciting prospect is the current development of large-scale atmospheric circulation models (Webster, 1977; Moriyama and Iwashima, 1980; Pollack *et al.*, 1981; Haberle *et al.*, 1982) whose numerical experiments can test many of the critical aspects of our present understanding of great dust storms. The interacting roles of topography, atmospheric waves, and dust heating require special attention. Ultimately, these models and the observations of the atmosphere of Mars will test our understanding of the nature and climatic stability of the Earth's own general atmospheric circulation. Specific examples are the quantitative determination of the factors governing the strength and extent of the zonally symmetric (Hadley) circulation, the relative roles of this circulation and of the longitudinally varying components (eddies) in controlling the transports of heat and minor constituents, and the effects of aerosols on the radiative balance of and the circulation above the polar regions.

However, confident extrapolation from the year-to-year seasonal cycle of dust to much longer climatic cycles will require more observational data than we now have. Synoptic coverage of the precursors of a great dust storm, of their horizontal and vertical expansion, and of the atmosphere's evolving static stability is needed to test quantitatively our understanding of the physical mechanisms combining to produce Martian great dust storms. One thing is certain: studies based on remotely sensed data of the Martian atmosphere or surface must contend with the atmospheric dust haze likely to be present. Future observers of Mars should be prepared to look through or to carefully characterize the nature of this Martian dust haze.

ACKNOWLEDGMENTS

I wish to thank T. Thorpe, P. Christensen, H.

Houben, R. Kahn, and R. Haberle for providing me with copies of their papers in advance of publication. This work was sponsored by the Planetary Atmospheres Program Office, NASA, and represents one phase of research carried out at the Jet Propulsion Laboratory, California Institute of Technology, under Contract NAS7-100, sponsored by the National Aeronautics and Space Administration.

REFERENCES

ANDERSON, E., AND C. LEOVY (1978). Mariner 9 television limb observations of dust and ice hazes on Mars. *J. Atmos. Sci.* **35,** 723–734.

BARNES, J. R. (1980). Time spectral analysis of midlatitude disturbances in the Martian atmosphere. *J. Atmos. Sci.* **37,** 2002–2015.

BARNES, J. R. (1981). Midlatitude disturbances in the Martian atmosphere: A second Mars year. *J. Atmos. Sci.* **38,** 225–234.

BAUM, W. A. (1973). The International Planetary Patrol program: An assessment of the first three years. *Planet. Space Sci.* **21,** 1511–1519.

BLUMSACK, S. L., P. J. GIERASCH, AND W. R. WESSELL (1973). An analytic and numerical study of the Martian planetary boundary layer over slopes. *J. Atmos. Sci.* **30,** 66–82.

BRIGGS, G. A., AND C. B. LEOVY (1974). Mariner 9 observations of the Mars north polar hood. *Bull. Amer. Meteorol. Soc.* **55,** 278–296.

BRIGGS, G. A., W. A. BAUM, AND J. BARNES (1979). Viking Orbiter imaging observations of dust in the Martian atmosphere. *J. Geophys. Res.* **84,** 2795–2820.

BROWN, R. A. (1974). *Analytical Methods in Planetary Boundary-Layer Modelling*. Wiley, New York.

CAPEN, C. F. (1971). Martian yellow clouds—Past and future. *Sky Telescope,* **41,** 117–120.

CAPEN, C. F. (1974). The Martian yellow cloud of July 1971. *Icarus* **22,** 345–362.

CAPEN, C. F., AND L. J. MARTIN (1971). The developing stages of the Martian yellow storm of 1971. *Bull.* **7,** No. 157, 211–216, Lowell Observatory, Flagstaff, Ariz.

CHAPMAN, S., AND R. S. LINDZEN (1970). *Atmospheric Tides*. Gordon & Breach, New York.

CHRISTENSEN, P. R. (1982). Martian dust mantling and surface composition: Interpretation of thermophysical properties. *J. Geophys. Res.*, in press.

CONRATH, B. J. (1975). Thermal structure of the Martian atmosphere during the dissipation of the dust storm of 1971. *Icarus* **24,** 36–46.

CONRATH, B. J. (1976). Influence of planetary-scale topography on the diurnal thermal tide during the 1971 Martian dust storm. *J. Atmos. Sci.* **33,** 2430–2439.

CONRATH, B., R. CURRAN, R. HANEL, V. KUNDE, W. MAGUIRE, J. PEARL, J. PIRRAGLIA, J. WELKER, AND T. BURKE (1973). Atmospheric and surface properties of Mars obtained by infrared spectroscopy on Mariner 9. *J. Geophys. Res.* **78,** 4267–4278.

DAVIES, D. W. (1979). Effects of dust on the heating of Mars' surface and atmosphere. *J. Geophys. Res.* **84,** 8289–8293.

FRENCH, R. G., AND P. J. GIERASCH (1979). The Martian polar vortex: Theory of seasonal variation and observations of eolian features. *J. Geophys. Res.* **84,** 4634–4642.

FRENCH, R. G., P. J. GIERASCH, B. D. POPP, AND R. J. YERDON (1981). Global patterns in cloud forms on Mars. *Icarus* **45,** 468–493.

GIERASCH, P. J. (1974). Martian dust storms. *Rev. Geophys. Space Phys.* **12,** 730–734.

GIERASCH, P. J., AND R. M. GOODY (1972). The effect of dust on the temperature of the Martian atmosphere. *J. Atmos. Sci.* **29,** 400–402.

GIERASCH, P. J., AND R. M. GOODY (1973). A model of a Martian great dust storm. *J. Atmos. Sci.* **30,** 169–179.

GIERASCH, P. J., AND C. SAGAN (1971). A preliminary assessment of Martian wind regimes. *Icarus* **14,** 312–318.

GIERASCH, P. J., P. THOMAS, R. FRENCH, AND J. VEVERKA (1979). Spiral clouds on Mars: A new atmospheric phenomenon. *Geophys. Res. Lett.* **6,** 405–408.

GIFFORD, F. A. (1964). A study of Martian yellow clouds that display movement. *Mon. Weather Rev.* **92,** 435–440.

GOLITSYN, G. S. (1973). On the Martian dust storms. *Icarus* **18,** 113–119.

GREELEY, R., R. LEACH, B. R. WHITE, J. D. IVERSEN, AND J. B. POLLACK (1980). Threshold wind speeds for sand on Mars: Wind tunnel simulations. *Geophys. Res. Lett.* **7,** 121–124.

HABERLE, R. M., C. B. LEOVY, AND J. B. POLLACK (1979). A numerical model of the Martian polar cap winds. *Icarus* **39,** 151–183.

HABERLE, R. M., C. B. LEOVY, AND J. B. POLLACK (1982). Some effects of global dust storms on the atmospheric circulation on Mars. *Icarus* **50,** 322–367.

HANEL, R., B. CONRATH, W. HOVIS, V. KUNDE, P. LOWMAN, W. MAGUIRE, J. PEARL, J. PIRRAGLIA, C. PRABHAKARA, B. SCHLACHMAN, G. LEVIN, P. STRAAT, AND T. BURKE (1972). Investigation of the Martian environment by infrared spectroscopy on Mariner 9. *Icarus* **17,** 423–442.

HESS, S. L. (1973). Martian winds and dust clouds. *Planet. Space Sci.* **21,** 1549–1557.

HOUBEN, H. (1982). A global Martian dust storm model. Submitted.

HUNT, G. E. (1979). Thermal infrared properties of the Martian atmosphere. 4. Predictions of the presence of dust and ice clouds from Viking IRTM spectral measurements. *J. Geophys. Res.* **84,** 2865–2874.

HUNT, G. E., E. A. MITCHELL, AND A. R. PETERFREUND (1980). The opacity of some local Martian dust storms observed by the Viking IRTM. *Icarus* **41**, 389–399.

JAMES, P. B., AND N. EVANS (1981). A local dust storm in the Chryse region of Mars: Viking Orbiter observations. *Geophys. Res. Lett.* **8**, 903–906.

JAMES, P. B., G. BRIGGS, J. BARNES, AND A. SPRUCK (1979). Seasonal recession of Mars' south polar cap as seen by Viking. *J. Geophys. Res.* **84**, 2889–2922.

JOSEPH, J. H., W. J. WISCOMBE, AND J. A. WEINMAN (1976). The delta-Eddington approximation for radiative flux transfer. *J. Atmos. Sci.* **33**, 2452–2459.

KAHN, R., R. GOODY, AND J. POLLACK (1981). The Martian twilight. *J. Geophys. Res.* **86**, 5833–5838.

KIEFFER, H. H. (1979). Mars south polar spring and summer temperatures: A residual CO_2 frost. *J. Geophys. Res.* **84**, 8263–8288.

LEOVY, C. B. (1981). Observations of Martian tides over two annual cycles. *J. Atmos. Sci.* **38**, 30–39.

LEOVY, C., AND Y. MINTZ (1969). Numerical simulation of the atmospheric circulation and climate of Mars. *J. Atmos. Sci.* **26**, 1167–1190.

LEOVY, C. B., AND R. W. ZUREK (1979). Thermal tides and Martian dust storms: Direct evidence for coupling. *J. Geophys. Res.* **84**, 2956–2968.

LEOVY, C., G. BRIGGS, A. YOUNG, B. SMITH, J. POLLACK, E. SHIPLEY, AND R. WILDEY (1972). The Martian atmosphere: Mariner 9 television experiment progress report. *Icarus* **17**, 373–393.

LEOVY, C. B., R. W. ZUREK, AND J. B. POLLACK (1973). Mechanisms for Mars dust storms. *J. Atmos. Sci.* **30**, 749–762.

LINDAL, G. F., H. B. HOTZ, D. N. SWEETNAM, Z. SHIPPONY, J. P. BRENKLE, G. V. HARTSELL, R. T. SPEAR, AND W. H. MICHAEL, JR. (1979). Viking radio occultation measurements of the atmosphere and topography of Mars: Data acquired during 1 Martian year of tracking. *J. Geophys. Res.* **84**, 8443–8456.

MARTIN, L. J. (1974). The major Martian yellow storm of 1971. *Icarus* **22**, 175–188.

MARTIN, L. J. (1975). North polar hood observations during Martian dust storms. *Icarus* **26**, 341–352.

MARTIN, L. J. (1976). 1973 dust storm on Mars: Maps from hourly photographs. *Icarus* **29**, 363–380.

MARTIN, T. Z., AND H. H. KIEFFER (1979). Thermal infrared properties of the Martian atmosphere. 2. The 15-μm band measurements. *J. Geophys. Res.* **84**, 2843–2852.

MARTIN, T. Z., AND R. W. ZUREK (1982). Mars: Atmospheric opacities inferred from Viking Orbiter Infrared Thermal Mapper data. In preparation.

MARTIN, T., A. PETERFREUND, E. MINER, H. KIEFFER, AND G. HUNT (1979). Thermal infrared properties of the Martian atmosphere. 1. Global behavior at 7, 9, 11, and 20 μm. *J. Geophys. Res.* **84**, 2830–2842.

MASS, C., AND C. SAGAN (1976). A numerical circulation model with topography for the Martian southern atmosphere. *J. Atmos. Sci.* **33**, 1418–1430.

MICHAUX, C. M., AND R. L. NEWBURN, JR. (1972). *Mars Scientific Model*. JPL Document No. 606-1, Jet Propulsion Laboratory, Pasadena, Calif.

MORIYAMA, S. (1975). Effects of dust on radiation transfer in the Martian atmosphere. II. Heating due to absorption of the visible solar radiation and importance of radiative effects of dust on the Martian meteorological phenomena. *J. Meteorol. Soc. Japan* **53**, 214–221.

MORIYAMA, S., AND T. IWASHIMA (1980). A spectral model of the atmospheric general circulation of Mars: A numerical experiment including the effects of the suspended dust and the topography. *J. Geophys. Res.* **85**, 2847–2860.

PALLUCONI, F. D., AND H. H. KIEFFER (1981). Thermal inertia mapping of Mars from 60°S to 60°N. *Icarus* **45**, 415–426.

PANG, K., AND J. M. AJELLO (1977). Complex refractive index of Martian dust: Wavelength dependence and composition. *Icarus* **30**, 63–74.

PANG, K., J. M. AJELLO, C. W. HORD, AND W. S. EGAN (1976). Complex refractive index of Martian dust: Mariner 9 ultraviolet observations. *Icarus* **27**, 55–67.

PETERFREUND, A. R. (1981). Visual and infrared observations of wind streaks on Mars. *Icarus* **45**, 447–467.

PETERFREUND, A. R., AND H. H. KIEFFER (1979). Thermal infrared properties of the Martian atmosphere. 3. Local dust clouds. *J. Geophys. Res.* **84**, 2853–2863.

PLESKOT, L. K., AND E. D. MINER (1981). Time variability of Martian bolometric albedo. *Icarus* **45**, 179–201.

POLLACK, J., D. COLBURN, R. KAHN, J. HUNTER, W. VAN CAMP, C. CARLSTON, AND M. WOLFE (1977). Properties of aerosols in the Martian atmosphere, as inferred from Viking Lander imaging data. *J. Geophys. Res.* **82**, 4479–4496.

POLLACK, J., D. COLBURN, F. M. FLASAR, R. KAHN, C. CARLSTON, AND D. PIDEK (1979). Properties and effects of dust particles suspended in the Martian atmosphere. *J. Geophys. Res.* **84**, 2929–2945.

POLLACK, J. B., C. B. LEOVY, P. W. GREIMAN, AND Y. MINTZ (1981). A Martian general circulation experiment with large topography. *J. Atmos. Sci.* **38**, 3–29.

RYAN, J. A., AND R. M. HENRY (1979). Mars atmospheric phenomena during major dust storms, as measured at surface. *J. Geophys. Res.* **84**, 2821–2829.

RYAN, J. A., AND R. D. SHARMAN (1981). Two major dust storms, one Mars year apart: Comparison from Viking data. *J. Geophys. Res.* **86**, 3247–3254.

RYAN, J. A., R. D. SHARMAN, AND R. D. LUCICH

(1981). Local Mars dust storm generation mechanism. *Geophys. Res. Lett.* **8,** 899–901.

SAGAN, C., AND J. B. POLLACK (1969). Windblown dust on Mars. *Nature* **223,** 791–794.

SAGAN, C., J. VEVERKA, P. FOX, R. DUBISCH, J. LEDERBERG, E. LEVINTHAL, L. QUAM, R. TUCKER, J. B. POLLACK, AND B. A. SMITH (1972). Variable features on Mars: Preliminary Mariner 9 TV results. *Icarus* **17,** 346–372.

SAGAN, C., D. PIERI, P. FOX, R. E. ARVIDSON, AND E. A. GUINNESS (1977). Particle motion on Mars inferred from the Viking Lander cameras. *J. Geophys. Res.* **82,** 4430–4438.

THOMAS, P., J. VEVERKA, S. LEE, AND A. BLOOM (1981). Classification of wind streaks on Mars. *Icarus* **45,** 124–153.

THORPE, T. E. (1973). Mariner 9 photometric observations of Mars from November 1971 through March 1972. *Icarus* **20,** 482.

THORPE, T. E. (1978). Viking Orbiter observations of the Mars opposition effect. *Icarus* **36,** 204–215.

THORPE, T. E. (1979). A history of Mars atmospheric opacity in the southern hemisphere during the Viking extended mission. *J. Geophys. Res.* **84,** 6663–6683.

THORPE, T. E. (1981). Mars atmospheric opacity effects observed in the northern hemisphere by Viking Orbiter imaging. *J. Geophys. Res.* **86,** 11419–11429.

TOON, O. B., J. B. POLLACK, AND C. SAGAN (1977). Physical properties of the particles composing the Martian dust storm of 1971–1972. *Icarus* **30,** 663–696.

VAN BLERKOM, D. J. (1971). The effect of haze on the visibility of Martian surface features. *Icarus* **14,** 235–244.

VEVERKA, J., P. GIERASCH, AND P. THOMAS (1981). Wind streaks on Mars: Meteorological control of occurrence and mode of formation. *Icarus* **45,** 154–166.

WEBSTER, P. J. (1977). The low-latitude circulation of Mars. *Icarus* **30,** 626–649.

ZUREK, R. W. (1976). Diurnal tide in the Martian atmosphere. *J. Atmos. Sci.* **33,** 321–337.

ZUREK, R. W. (1978). Solar heating of the Martian dusty atmosphere. *Icarus* **35,** 196–208.

ZUREK, R. W. (1981). Inference of dust opacities for the 1977 Martian great dust storms from Viking Lander 1 pressure data. *Icarus* **45,** 202–215.

ZUREK, R. W., AND C. B. LEOVY (1981). Thermal tides in the dusty Martian atmosphere: A verification of theory. *Science* **213,** 437–439.